SEMI-BLIND JOINT SUPER-RESOLUTION/SEGMENTATION OF 3D TRABECULAR BONE IMAGES BY A TV BOX APPROACH

Françoise Peyrin[1,2]*, Alina Toma* [1]*, Bruno Sixou* [1]*, Loïc Denis* [3]*, Andrew Burghardt*[4]*, Jean-Baptiste Pialat* [5]

[1] CREATIS, INSA de Lyon, Inserm U1044, CNRS UMR 5220,
Université Lyon 1, Université de Lyon, 69621 Villeurbanne, France
[2] ESRF, Imaging Group, 38043 Grenoble Cedex, France
[3] LaHC, CNRS UMR 5516, Université de Saint-Etienne, 42000 Saint-Etienne, France
[4] Musculoskeletal Quantitative Imaging Research Group, Department of Radiology and Biomedical Imaging, University of California, San Francisco, CA, 94158, USA
[5] Inserm U1033; Université de Lyon, Hospices Civils de Lyon, 69437 Lyon, France

ABSTRACT

The investigation of bone fragility diseases, as osteoporosis, is based on the analysis of the trabecular bone micro-architecture. The aim of this paper is to improve the *in-vivo* trabecular bone segmentation and quantification by increasing the resolution of bone micro-architecture images. We propose a semi-blind joint super-resolution/segmentation approach based on a Total Variation regularization with a convex constraint. A comparison with the bicubic interpolation method and the non-blind version of the proposed method is shown. The validation is performed on blurred, noisy and down-sampled 3D synchrotron micro-CT bone images. Good estimates of the blur and of the high resolution image are obtained with the semi-blind approach. Preliminary results are obtained with the semi-blind approach on real HR-pQCT images.

Index Terms— Semi-blind super-resolution, segmentation, Total Variation, 3D micro-CT, bone micro-architecture.

1. INTRODUCTION

In the context of osteoporosis, the trabecular bone micro-architecture is known to be an important determinant of bone strength. However, its analysis from *in-vivo* CT images remains most of the time limited due to the lack of spatial resolution. This is related to the very small size of the trabeculae (mean thickness of about 120 μm) compared to the resolution of CT scanners.

New High Resolution peripheral Quantitative CT (HR-pQCT) devices with improved spatial resolution are currently available in a number of pilot research sites in the world [3,6]. This technique typically provides 3D images of bone with an isotropic voxel size of 82 μm.

After binarization, quantitative parameters of trabecular bone architecture can be extracted. They include morphometric parameters such as the bone volume to total volume ratio, mean trabecular thickness, mean trabecular spacing, as well as nonmetric parameters like the density of connectivity. Nevertheless, by comparing this technique to micro-CT at higher spatial resolution, it was shown that some of these parameters were particularly sensitive to the segmentation [10]. Then, since the spatial resolution of this system remains close to the trabeculae size, the segmentation of trabecular bone continues to be an issue.

In this paper, we will present our investigations to improve the quality of trabecular bone micro-CT images based on super-resolution techniques. Conversely to standard super-resolution methods, our input is a single low spatial resolution image for which we expect to recover a higher spatial resolution image. Since the final goal is to obtain a binary image of trabecular bone, we consider solving the joint super-resolution/segmentation problem.

We shall first summarize the approach developed using a prior based on Total Variation with a convex relaxation of the binary constraint (TVbox). We provided an algorithm based on Alternating Direction Method of Multipliers (ADMM) algorithm, which is one of the state of-the-art method for TV regularization [1,14,21]. First results were obtained on experimental micro-CT images used as ground truth and degraded with a known blur kernel [20]. Since the trabecular bone images are displaying quasi-binary structures, a TV prior was preferred. The results show an improvement in images and particularly a better preservation of connectivity.

However, when considering real data, the problem is more complex since the blurring kernel is not known and may be difficult to estimate. Several methods have been proposed for the simultaneous recovery of the image and of the

This work was supported by the LABEX PRIMES (ANR-11-LABX-0063) of Université de Lyon, within the program "Investissements d'Avenir" (ANR-11-IDEX-0007) operated by the French National Research Agency (ANR).

point spread function (PSF), like bayesian methods [2, 13], Tikhonov regularization [22] or Total Variation (TV) regularization [2, 7, 11]. Estimating the unknown image and some partially known PSF is referred to as semi-blind deconvolution [9, 12].

Thus, we finally address the problem of semi-blind joint super-resolution/segmentation aiming at estimating both the segmented super-resolved image and the gaussian blurring kernel. Preliminary results on experimental HR-pQCT images are presented.

2. JOINT SUPER-RESOLUTION / SEGMENTATION

2.1. Direct problem

The direct problem is formulated as follows. Let $\boldsymbol{g} \in \mathbb{R}^N$ be the observed 3D low-resolution discrete image with N voxels. Let $\boldsymbol{f} \in \mathbb{R}^{N'}$ with $N' = Np^3$, be the super-resolved image where p is the over-sampling factor. The relationship between $\boldsymbol{f}$ and $\boldsymbol{g}$ is given by a linear operator, $\boldsymbol{A}$, combining the effects of down-sampling and blurring. By assuming that the image is corrupted by an additive noise, the direct problem can be expressed as :

$$\boldsymbol{g} = \boldsymbol{A}\boldsymbol{f} + \boldsymbol{n}, \tag{1}$$

where $\boldsymbol{n}$ is a centered Gaussian noise with standard deviation σ_n.

2.2. Proposed minimization

In order to solve this inverse problem, we first proposed to introduce a TV prior on the image. The conventional TV regularization scheme consists in minimizing the following functional:

$$J(\boldsymbol{f}) = \frac{\mu}{2} \left\| \boldsymbol{A}\boldsymbol{f} - \boldsymbol{g} \right\|_2^2 + \|\nabla \boldsymbol{f}\|_1. \tag{2}$$

where μ is a regularization parameter. Since our final aim is to combine super-resolution and segmentation, we assume that the segmented super-resolved image is binary and takes two values, c_0 and c_1. Let $\mathcal{B} = \{c_0, c_1\}^{N'}$, the minimization problem becomes:

$$\hat{\boldsymbol{f}} = \arg\min\{J(\boldsymbol{f}), \boldsymbol{f} \in \mathcal{B}\}. \tag{3}$$

Convexified models obtained by relaxation of the binary constraint have often been considered for segmentation tasks [4, 5, 18]. We used the same type of method and we proposed to solve an approximate minimization problem by relaxing the binary constraint and searching for a quasi-binary graylevel image with graylevels in the range $[c_0, c_1]$ [20]. This yields to a convex problem:

$$\hat{\boldsymbol{f}} = \arg\min\{J(\boldsymbol{f}), \boldsymbol{f} \in [c_0, c_1]^{N'}\}. \tag{4}$$

This problem was solved by using an ADMM algorithm. The augmented Lagrangian was written as :

$$\begin{aligned}\mathcal{L}_{\mathrm{A}}(\boldsymbol{f}, \{\boldsymbol{h}_i\}, \boldsymbol{k}, \{\boldsymbol{\lambda}_i\}, \boldsymbol{\lambda_C}) = \frac{\mu}{2} \left\| \boldsymbol{A}\boldsymbol{f} - \boldsymbol{g} \right\|_2^2 + \sum_i \|\boldsymbol{h}_i\| \\ + \sum_i \left[\frac{\beta}{2} \|\boldsymbol{h}_i - \boldsymbol{D}_i \boldsymbol{f}\|^2 - \boldsymbol{\lambda}_i^{\mathrm{t}} (\boldsymbol{h}_i - \boldsymbol{D}_i \boldsymbol{f}) \right] \\ + \boldsymbol{I_C}(\boldsymbol{k}) + \frac{\beta}{2} \|\boldsymbol{k} - \boldsymbol{f}\|_2^2 - \boldsymbol{\lambda}_{\boldsymbol{C}}^t (\boldsymbol{k} - \boldsymbol{f})\end{aligned} \tag{5}$$

with $\boldsymbol{\lambda}_i$ the Lagrange multipliers for the i^{th} equality constraint, $\boldsymbol{\lambda_C}$ the Lagrange multiplier for convex constraint, β the augmented Lagrangian parameter and $\boldsymbol{I_C}$ is the indicator function of the convex set $\mathrm{C} = [c_0, c_1]^{N'}$. The auxiliary $\boldsymbol{h}_i$ and $\boldsymbol{k}$ are used to take into account the two constraints. The optimal image is obtained by successive minimizations of the Lagrangian with respect to $\boldsymbol{f}$, the auxiliary variables and to the Lagrange multipliers [20].

3. SEMI-BLIND JOINT SUPER-RESOLUTION/ SEGMENTATION

In this work, we have extended the non-blind approach presented in [20] to a semi-blind estimation of the blurring kernel and of the high resolution segmented image.

3.1. Direct problem

In the general case, solving the blind super-resolution problem requires to estimate both $\boldsymbol{f}$ and the blurring operator from (1). In this first approach, we assume that the blur is isotropic and can be represented by a 3D Gaussian kernel:

$$\alpha(x, y, z) = \alpha_\sigma(x)\alpha_\sigma(y)\alpha_\sigma(z) \tag{6}$$

where $\alpha_\sigma(x)$ is the 1D Gaussian kernel of standard deviation σ. The problem in now reformulated as a semi-blind problem:

$$\{\hat{\boldsymbol{f}}, \sigma\} = \arg\min\{J(\boldsymbol{f}, \sigma), \boldsymbol{f} \in [c_0, c_1]^{N'}, \sigma > 0\}. \tag{7}$$

where $J(\boldsymbol{f}, \sigma)$ includes the dependence of the blurring kernel on σ.

3.2. Minimization algorithm

We note that the cost function is convex with respect to $\boldsymbol{f}$, but not convex with respect to the standard deviation σ. Thus, in order to find the solution $\{\hat{\boldsymbol{f}}, \sigma\}$ that minimizes the cost function (7), we apply the alternating minimization scheme:

Step 0: Choose a starting sigma value $\sigma^{(0)}$, t=0

Step 1: t=t+1, Refine the image:

$$\boldsymbol{f}^{(t)} = \underset{\boldsymbol{f} \in [c_0, c_1]^{N'}}{\arg\min} \ \frac{\mu}{2} \left\| \boldsymbol{A}^{(t-1)} \boldsymbol{f} - \boldsymbol{g} \right\|_2^2 + \|\nabla \boldsymbol{f}\|_1 \tag{8}$$

where $\boldsymbol{A}^{(t-1)}$ is the direct operator at the step t-1.

Step 2: Refine the blur:

$$\sigma^{(t)} = \arg\min_{\sigma} \left\| \boldsymbol{A}(\sigma)\boldsymbol{f}_{01}^{(t)} - \boldsymbol{g} \right\|_2^2 \quad (9)$$

where $\boldsymbol{f}_{01}$ is the binary version of $\boldsymbol{f}$.

Step 3: Go to step 1 until convergence.

We perform the minimization of (8) with the ADMM scheme presented in [20]. At step 2, the Newton method is applied for obtaining the solution $\sigma^{(t)}$. A local optimum is obtained since the regularization functional is not a convex function of σ.

4. NUMERICAL EXPERIMENTS

4.1. Experiments on simulated images

We first consider simulations based on experimental micro-CT images of bone samples artificially blurred and under-sampled. Human bone samples (cylinder core of 10 mm) were imaged using parallel-beam synchrotron micro-CT at 10 μm. The images were reconstructed from 1500 2D projections using the Filtered back projection algorithm [19] and further resampled at 20 μm. These 3D images considered as ground truths, were blurred with a Gaussian kernel with a standard deviation $\sigma = 2.4$ and down-sampled at 40 μm (p=2). Gaussian noise level with standard deviation $\sigma_n = 0.1$ was added to the image. The method was tested on a Volume of Interest (VOI) of $(328)^3$ voxels. Considering the bimodal histogram of the ground truth volume, the binary version of it was obtained with Otsu's method [17].

The semi-blind super-resolution/segmentation method was applied using the TV regularization with box constraints. An extensive sweeping of the regularization parameters was performed in order to show that this method can be useful to recover the high resolution segmented ground truth. For a fixed regularization parameter μ, the parameter β is chosen in order to have the fastest decrease of the regularization functional.

For each method, the regularization parameter μ chosen is the one that maximizes the DICE value [8] between the binary ground truth and the segmented reconstructed volume obtained with the threshold 0.5. For comparison reasons, the low resolution volume and the bicubic interpolation volume were segmented with Otsu's method. The performance of the methods was measured considering the DICE value and also the quantitative bone micro-architecture parameters such as the bone volume to total volume (BVTV in %), the Euler number (χ) [16] and the density of connectivity (dconn in mm^{-3}) [15].

The results are presented in Figures 1-2 and Table 1. Slices and a 3D rendering of a cropped volume are displayed.

4.2. Experiments on real images

We present preliminary work on experimental data. 3D images of human radius samples were acquired on a HR-pQCT system from 750 projections and reconstructed at an isotropic voxel size of 82 μm. The same samples were also scanned using a micro-CT system providing 3D images at 24 μm. The HR-pQCT images were registered to the ground truth micro-CT images. Figure 3 (a) and (b) show a region of interest (ROI) within the micro-CT image resampled at 41 μm and the original HR-pQCT image at 82 μm. With real data, only the semi-blind TVbox approach could be applied. Figures 3 (c) and (d) respectively show the bicubic interpolated slice and a first result of the super-resolved TVbox image with the up-sampled factor p=2. The best results were obtained with the initial value of the $\sigma^{(0)}$=0.5. We may note that the Dice index is increased with the TVbox method (0.7 versus 0.61).

5. CONCLUSION

In this paper, we proposed a semi-blind joint super-resolution/ segmentation method based on the Total Variation regularization with convex constraint and ADMM minimization for improving the trabecular bone micro-structure quantification from micro-CT volumes. We compared this semi-blind TVbox approach with the standard interpolation method in terms of DICE and structural parameters. For artificially deteriorated Synchrotron images a comparison with the non-blind TVbox method is performed. We showed that our semi-blind method is improving the structural parameters compared to the original one and also that we efficiently estimate the blur kernel. It outperforms clearly the interpolation method. Preliminary results show that the approach can be applied to real HR-pQCT images for which we have a ground truth image. In further work, we shall address the optimization of the parameters of the algorithm and particularly the choice of c_0 and c_1 used for box constraints. We will also consider anisotropic and spatially varying blurring kernel. Other segmentation methods to obtain the binary version of the low resolution image and bicubic interpolation will be investigated.

REFERENCES

[1] M. Afonso, J. Bioucas-Dias and M. Figueiredo, "Fast image recovery using variable splitting and constrained optimization", *IEEE Trans. Image Process.*, vol. 19, pp. 2345-2356, 2010.

[2] S.D.Babacan, R.Molina and A.K.Katsaggelos, "Variational Bayesian blind deconlution using a total variation prior", *IEEE Transactions on Image Processing*, vol. 18, pp.12-26, 2009.

[3] S. Boutroy, M. L. Bouxsein, F. Munoz and P. D. Delmas, "In vivo assessment of trabecular bone microarchitecture by high-resolution peripheral quanti-

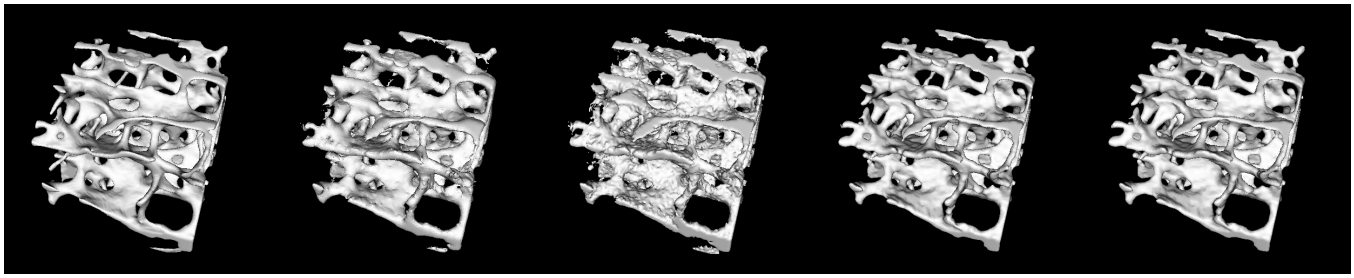

(a) Ground-truth volume (b) Low resolution volume (c) Bicubic interpolation (d) TVbox regular. (e) semi-blind TVbox regular.

Fig. 1. Comparison of 3D restoration methods on experimental synchrotron volume.

(a) Ground-truth slice (b) Low resolution slice (c) Bicubic interpolation (d) TVbox regular. (e) semi-blind TVbox regular.

Fig. 2. Slice of the restored experimental synchrotron volume.

Parameter	Ref.	Low resolution	Bicubic Interpolation	TVbox	semi-blind TVbox
DICE	1	-	0.773	0.908	0.915
Euler no.	-1211	4888	11201	-722	-753
dconn (mm^{-3})	4.86	16.61	11.98	4.20	4.22
BVTV (%)	11.07	16.48	16.38	11.50	11.45

Table 1. Quantitative parameters.

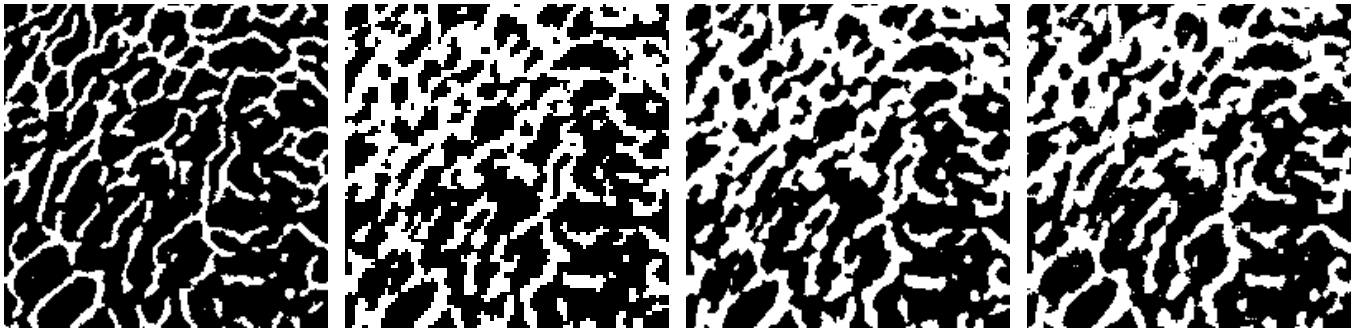

(a) Ground-truth micro-CT slice (b) HR-pQCT slice (c) Bicubic interpolation (d) semi-blind TVbox regular.

Fig. 3. Slice of the restored HR-pQCT volume.

tative computed tomography", *J. Clin. Endocrinol. Metab.*, vol. 90, no. 12, pp. 6508-15, 2005.

[4] X. Bresson, S. Esedoglu, P. Vandergheynst, J. P. Thiran and S. Osher, Fast global minimization of the active contour/snake model, *Journal of Mathematical Imaging and Vision*, **28** (2007) 151-167.

[5] E. S. Brown, T. F. Chan and X. Bresson, Completely convex formulation of the Chan-Vese image segmentation model, *International Journal of Computer Vision*, (2011) 1-19.

[6] A. J. Burghardt, J.-B. Pialat, G. J. Kazakia, S. Boutroy, K. Engelke, J. M. Patsch, A. Valentinitsch, D. Liu, E. Szabo, C. E. Bogado, M. B. Zanchetta, H. A. McKay, E. Shane, S. K. Boyd, M. L. Bouxsein, R. Chapurlat, S. Khosla, and S. Majumdar, "Multicenter precision of cortical and trabecular bone quality measures assessed by high-resolution peripheral quantitative computed tomography", *J Bone Miner Res*, vol. 28, no. 3, pp. 524-36, 2013.

[7] T. F. Chan and C. K. Wong, "Total variation blind deconvolution", *IEEE Transactions on Image Processing*, vol. 7, pp.370-375, 1998.

[8] L. R. Dice, "Measures of the amount of ecologic association between species", *Ecology*, vol. 26, no.3, pp. 297-302, Jul. 1945.

[9] N. P. Galatsanos, V. Z. Mesarovic, R. Molina, A. K. Katsaggelos, J. Mateos, "Hierarchical Bayesian image restoration from partially known blurs", *IEEE Trans. Image Process.*, vol.9, pp. 1784-1797, 2000.

[10] M. Krause, O. Museyko, S. Breer, B. Wulff, C. Duckstein, E. Vettorazzi, C. Glueer, K. Pschel, K. Engelke, and M. Amling, "Accuracy of trabecular structure by HR-pQCT compared to gold standard CT in the radius and tibia of patients with osteoporosis and long-term bisphosphonate therapy", *Osteoporos Int*, vol. 25, no. 5, pp. 1595-606, 2014.

[11] H. Liao and M. K. Ng, "Blind deconvlution using generalized cross-validatin approach to regularization parameter estimation", *IEEE Transactions on Image Processing*, vol. 20, pp. 670-680, 2011.

[12] R. Molina, "On the hierarchical Bayesian approach to image restoration: applications to astronomical images", *IEEE Trans. Patterns Anal. Mach. Intell.* , vol.16, pp. 1122-1128, 1994.

[13] R. Molina, J. Mateos an A. K. Katsaggelos, "Blind deconvolution using a variational approach to parameter, image and blur estimation", *IEEE Transactions on Image Processing*, vol.15, pp. 3715-3727, 2006.

[14] MK. Ng, P. Weiss and X. Yuan, "Solving constrained total-variation image restoration and reconstruction problems via alternating direction mehthods", *SIAM J. Sci. Comput.*, vol. 32, pp. 2710-2736, 2010.

[15] A. Odgaard, "Three-dimensional methods for quantification of cancellous bone architecture", *Bone*, vol 20, no. 4, pp. 315-28, 1997.

[16] J. Ohser, W. Nagel and K. Schladitz, "Miles formulae for boolean models observed on lattices", *Image Anal. Stereol.*, vol. 28, no. 2, pp. 77-92, 2009.

[17] N. Otsu, "A threshold selection method from gray-level histograms", *IEEE Trans. Sys., Man. Cyber.*, vol. 9, no.1, pp. 62-66, 1979.

[18] G. Paul, J. Cardinale and I. F. Sbalzarini, "Coupling image restoration and segmentation: A generalized linear model/Bregman perspective", *Int. J. Comput. Vis.*, vol. 104, pp. 69-93, 2013.

[19] M. Salome, F. Peyrin, P. Cloetens, C. Odet, A. M. Laval-Jeantet, J. Baruchel and P. Spanne, "A synchrotron radiation microtomography system for the analysis of trabecular bone samples", *Med. Phys.*, vol. 26, no. 10, pp. 2194-2204, Oct. 1999

[20] A. Toma, L. Denis, B. Sixou, J.-B. Pialat and F. Peyrin, "Total variation Super-resolution for 3D trabecular bone micro-structure segmentation", EUSIPCO, pp. 2220-2224, 2014

[21] J. Yang, W. Yin, Y. Zhang and Y. Wang, "A fast algorithm for edge-preserving variational multichannel image restoration", *SIAM J. Imaging Sci.*, vol. 2, pp. 569-592, 2008.

[22] Y. You and M. Kaveh, "A regularization approach to joint blur identification and image restoration", *IEEE Transactions on Image Processing*, vol.5, pp. 416-427, 1996.